Modulating LOV Domain Photodynamics with a Residue Alteration outside the Chromophore Binding Site

Sang-Hun Song,[†] Peter L. Freddolino,[‡,∥] Abigail I. Nash,[§] Elizabeth C. Carroll,[†] Klaus Schulten,[‡] Kevin H. Gardner,[§] and Delmar S. Larsen[†,*]

[†]Department of Chemistry, University of California, One Shields Avenue, Davis, California 95616, United States
[‡]Beckman Institute, University of Illinois, 405 North Mathews Avenue, Urbana, Illinois 61801, United States
[§]Departments of Biochemistry and Pharmacology, University of Texas Southwestern Medical Center, 5323 Harry Hines Boulevard, Dallas, Texas 75390, United States

S *Supporting Information*

ABSTRACT: Phototropins, a class of light-activated protein kinases, are essential for several blue light responses in plants and algae, including phototropism. These proteins contain two internal light, oxygen, and voltage sensitive (LOV) domains, which bind flavin chromophores and undergo a reversible photochemical formation of a cysteinyl−flavin adduct as part of the light sensing process. While the photodynamic properties of such photosensory domains are dictated by interactions between the chromophore and surrounding protein, more distant residues can play a significant role as well. Here we explore the role of the Phe434 residue in the photosensory response of the second LOV domain of *Avena sativa* phototropin 1 (AsLOV2), a model photochemical system for these LOV domains. Phe434 is more than 6 Å from the FMN chromophore in AsLOV2; nevertheless, an F434Y point mutation is likely to change several structural features of the chromophore binding site, as we demonstrate using molecular dynamics simulations. Transient absorption signals spanning 15 decades in time were compared for wild-type AsLOV2 and the F434Y mutant, showing that the latter has significantly altered photodynamics, including (i) a faster intersystem crossing leading to triplet formation on a nanosecond time scale, (ii) biphasic formation of adduct-state kinetics on the microsecond time scale, and (iii) greatly accelerated ground-state recovery kinetics on a second time scale. We present mechanistic models that link these spectroscopic differences to changes in the configuration of the critical cysteine residue and in the chromophore's accessibility to solvent and oxygen according to MD trajectories and purging experiments. Taken together, these results demonstrate the importance of residues outside the chromophore-binding pocket in modulating LOV domain photodynamics.

Photosensory receptor proteins, which transduce the energy from the absorption of photons into useful physiological functions, play an essential role for most organisms in the adjustment of their behavior and metabolism in response to the quantity and quality of light in their environment. Such proteins rely on small molecule chromophores that undergo light-dependent configurational changes to generate biological responses through biochemical signal transduction pathways.[1,2] From many perspectives, photoreceptor proteins are ideal systems for studying signal perception and transduction activity, (i) because they can be triggered with short pulses of light and (ii) because their signaling activity can be followed directly with spectroscopic techniques.

Light-sensing systems encompass multiple families of proteins, including the LOV (light, oxygen, and voltage sensitive) domains, BLUF (blue light sensors utilizing flavin) domains, cryptochromes, photoactive yellow protein, rhodopsins, and phytochromes.[1,3−8] The phototropin, BLUF, and cryptochrome families utilize flavin chromophores that absorb light to initiate photoactivity. In cryptochromes and BLUF domains, the flavin chromophore is noncovalently bound as a flavin adenine dinucleotide (FAD),[9,10] whereas most LOV domains bind flavin mononucleotide (FMN) chromophores. Examples of the latter domains include the tandem LOV1 and LOV2 domains within phototropins, a class of light-activated serine/threonine kinases

found in plants and algae.[11] These proteins mediate several classical blue light responses in plants, including phototropism (plant growth toward light sources), stomatal opening, chloroplast movement, and rapid inhibition of stem growth.[12] Since their initial characterization in phototropins, LOV domains have been found in a wide variety of proteins from plants, algae, fungi, and bacteria.[13]

In contrast to the rapid (200 fs to 200 ps) photoisomerization mechanisms in the photoactive yellow protein (PYP),[14] rhodopsin,[15] and phytochrome[8,16−18] families (<10 ps),[16] the primary photochemistry in LOV domains involves the much slower formation of a protein−chromophore adduct (several microseconds) between a conserved cysteine residue and the flavin C4a atom. While the molecular mechanisms of adduct formation remain somewhat controversial,[19−21,35] with the latest evidence favoring a radical pair mechanism,[22] they are preceded by the fast generation (<3 ns) of a reactive triplet state populated via intersystem crossing (ISC) from the initial photoexcited singlet state (Figure 1). The reactive triplet persists for several microseconds before generating the metastable photoadduct with a new covalent bond between FMN and a nearby cysteine residue, which is Cys450 in the model LOV system AsLOV2
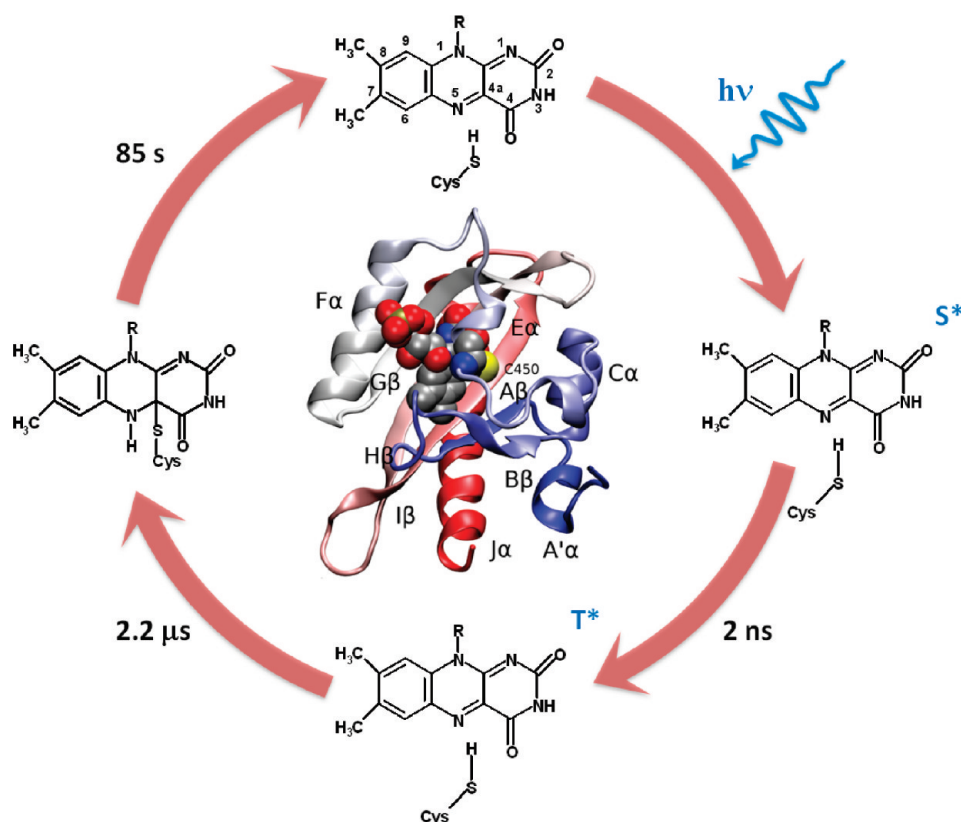
Figure 1. Primary steps in the wild-type AsLOV2 photocycle. The dark-adapted population (top) has the FMN molecule (with IUPAC atomic labels) bound to the protein via noncovalent interactions. Upon photoexcitation, FMN is promoted to an excited singlet state (right), which persists for 2 ns before generating the excited triplet state (bottom). The FMN triplet state persists for 2.2 μs before forming an adduct between the sulfur on Cys450 and C4a on FMN (left). The adduct is stable for 85 s before completing the photocycle by recovering the dark-adapted population. The inset shows a ribbon diagram of the dark-adapted AsLOV2 structure[29] with secondary structure elements labeled and a space-filling view of FMN.

(LOV2 domain of *Avena sativa* phototropin 1) (Figure 2).[19] The photoadduct alters the surrounding protein structure, leading to conformational changes that trigger biological responses. For AsLOV2, adduct formation results in the unfolding of the Jα helix that is located immediately C-terminal to the LOV domain,[23,24] generating the putative phototropin signaling state. The photoadduct recovers back to the dark-adapted singlet ground state through a light-independent mechanism on a time scale between seconds and hours, depending on the specific LOV domain.[19,25−27]

The flavin chromophore within a LOV domain is noncovalently bound to the protein via hydrophobic interactions complemented by a network of hydrogen bonds involving multiple amino acids (Scheme 1).[28] Each of these amino acids potentially plays a role in adjusting the photochemical properties of the receptor via their specific interactions with the FMN chromophore, surrounding protein, or both. For example, the side chain of Gln513 donates a hydrogen bond to O4 of FMN in the dark-state AsLOV2 structure.[29] Although Gln513 does not directly interact with the Cys450 residue involved in the photoadduct, mutations at Gln513 can strongly affect the observed photocycle dynamics, as demonstrated by the 15-fold slower ground-state recovery kinetics of the Q513L mutant.[30] Similarly, Ile427 and Asn449 stabilize the cysteinyl−flavin photoadduct via their van der Waals contacts with Cys450,[29] as argued by the faster observed adduct decay kinetics observed in an I427V mutant AsLOV2 that removes this favorable interaction.[31]

While Ile427, Asn449, and Gln513 have been identified as being important for LOV photocycling by either physical proximity[28] or random mutagenesis,[31] as have certain other residues by mechanism-based approaches,[32] there is a need for further rationally predicted mutations that alter LOV domain photochemistry. Molecular dynamics (MD) simulations provide a useful computational route to such predictions, via their ability to explore conformations that are functionally critical but difficult to characterize by X-ray crystallography or solution NMR spectroscopy. An example of this is provided by recent MD simulations of wild-type AsLOV2 that suggest that formation of the cysteinyl−flavin photoadduct forces the Gln513 side chain to rotate away from the flavin and break the hydrogen bond to the FMN O4 atom observed in the dark state (Figure 2A).[33] This alteration of the Gln513 conformation tilts the Iβ strand and destabilizes the interface with the Jα helix by introducing a bulge into the binding surface and by changing the conformational distribution of the Hβ−Iβ loop (Figure 1, inset).[33,34]

Given the nature of the structural changes to Gln513 observed in the light-induced state, we hypothesized that the introduction of a hydrogen bond-donating residue into the FMN binding pocket "above" the plane of the isoalloxazine ring system (in the direction of Cys450) would result in a flipped rotamer of Gln513 that would persist in the dark state and yield a constitutively active LOV2 domain. On the basis of structural analysis, three mutations were selected to achieve this goal: V416T, F434Y, and
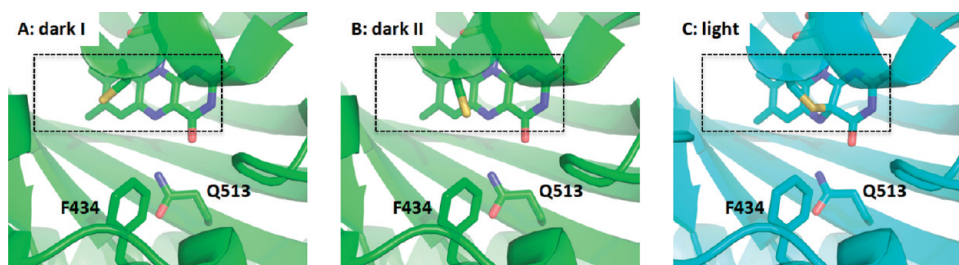
Figure 2. Protein structure surrounding the FMN cofactor in the wild-type AsLOV2 domain, as identified in crystal structures.[22] (A) Dark structure with Cys450 in conformation I. (B) Dark structure with conformation II. (C) Light-state adduct. The Eα helix contains the adduct-forming Cys450 residue, while Gln513 in the Iβ strand makes hydrogen bonds with O4 of the FMN isoalloxazine ring in the dark state. Phe434 on the Cα helix interacts with Gln513 through Asn414.

Scheme 1[a]
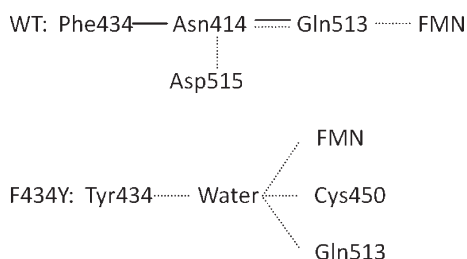
[a] Phe434 in the wild type and Tyr434 in the mutant are in ncontact with other amino acid residues, yielding hydrogen bonds to FMN. Solid lines denote van der Waals interactions and dashed lines hydrogen bonds. In the light-induced state, a structural change induces breakage of the hydrogen bond between Asn414 and Asp515.

L453T. All three mutants were investigated with MD simulations in both the dark and light states and subsequently overexpressed in *Escherichia coli* and purified (Supporting Information). While the V416T variant appeared to be unperturbed from the wild type both in MD simulations and on the basis of similarities in NMR and visible absorbance spectra, and the L453T mutant was insufficiently stable for biophysical characterization (data not shown), aspects of the F434Y mutation-containing protein warranted further investigation. Notably, simulations of the F434Y mutant showed altered Gln513 behavior and the rotameric distribution of the photoreactive Cys450 residue that suggested that this variant might demonstrate significant changes in photodynamic properties. It should be noted that while classical molecular dynamics simulations cannot treat the changes in electronic structure involved in the photoreaction itself, they can provide crucial data about the environment of the flavin chromophore in both the dark and light states as demonstrated here.

Presented here is a combined simulation and experimental study that explores the influence of the F434Y mutation on the photodynamics of the AsLOV2 domain extending over 15 decades in time. Atomistic MD simulations provide detailed information about chromophore binding pocket dynamics and energetics, including the conformational kinetics of nearby residues. We also resolve water and oxygen accessibilities to the binding pocket. Experimentally, the formation and decay kinetics of both the triplet state of the photoexcited FMN cofactor and the photoadduct species were resolved with a combination of absorption spectroscopy techniques sensitive to ultrafast (femtoseconds to nanoseconds), fast (microseconds), and slow (seconds) photodynamics.

■ MATERIALS AND METHODS

The details of sample preparation, experimental techniques, and computational approaches are described in the Supporting Information and are briefly summarized here. The ultrafast (femtoseconds to nanoseconds) photodynamics in both the dark and light states for each AsLOV2 variant studied were resolved using atomistic molecular dynamics simulations with three 200 ns trajectories in each case for the F434Y mutant that are compared to five 200 ns trajectories in each state from a recently completed study of wild-type AsLOV2.[33] Solution NMR experiments were performed on Varian Inova 600 and 800 MHz spectrometers at 25 °C. The transient absorption signals resolving the ultrafast dynamics were measured with an amplified mode-locked Ti:Sapphire laser spectrometer, generating both 50 fs, 400 nm excitation pulses and broadband visible probe pulses. The photodynamics extending from 10 ns to 20 μs were collected with an ancillary flash photolysis setup using 50 fs, 400 nm laser pulses for excitation and a 640 nm CW laser diode as the probe.

■ RESULTS

Molecular Dynamics Simulations. A number of experimental and computational studies have identified motion of Gln513 as a key step in activation of the LOV domain after the photoreaction.[20,24,28,34−40] While it has generally been assumed that the rotation of Gln513 that allows hydrogen bonding with the newly protonated N5 is the key structural change for activation, recent MD simulations of wild-type AsLOV2 (using the same structures as in this study) suggest that this hydrogen bond is only transiently populated (present in <10% of time steps).[33] Similar results had been previously obtained for a LOV2 domain from *Adiantum capillus-veneris* phy3,[34] and notably, a high-resolution crystal structure of AsLOV2 failed to exhibit formation of this hydrogen bond upon illumination.[29] Instead, the primary structural change observed in the MD simulations[33] of the light-induced state is one in which Gln513 rotates away from FMN altogether and in many cases is replaced by a water interacting directly with FMN at O4 and/or N5. This light-induced rotation of Gln513 was correlated with broader structural changes such as tilting of the Iβ strand that contribute to dissociation of the Jα helix.

In addition to the observed changes in the conformation of Gln513 (Supporting Information), the F434Y mutation introduces a water binding site adjacent to FMN that is similar to light-induced structural changes to be reported elsewhere.[33] Volumetric
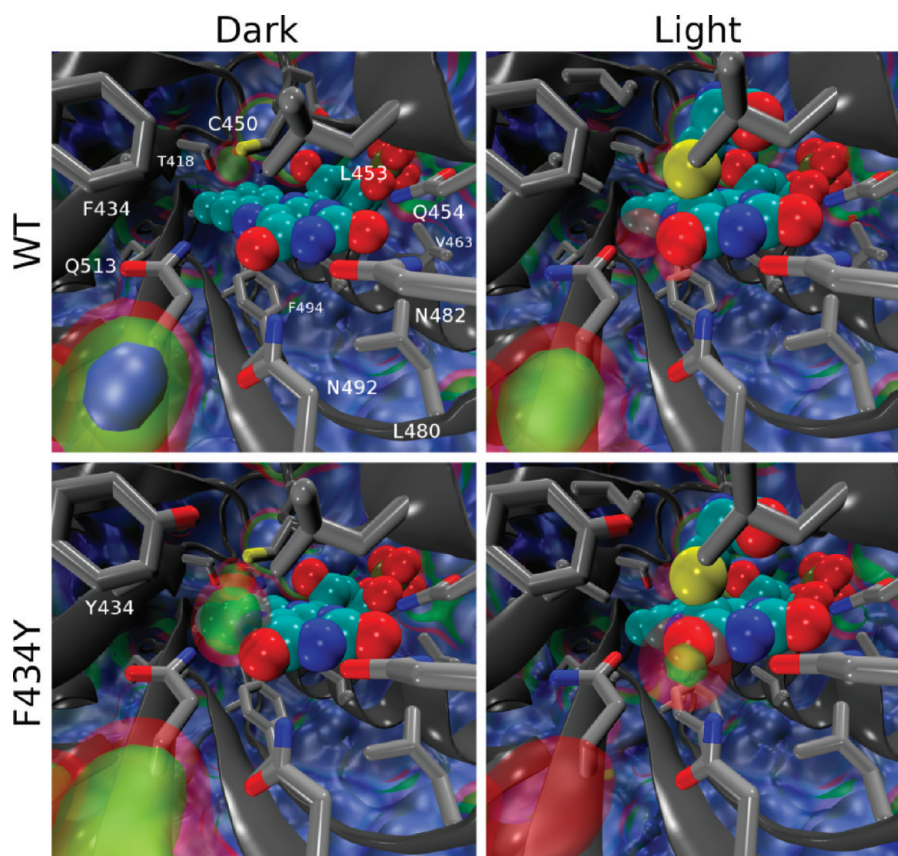
Figure 3. Volumetric maps showing water occupancy in and around the FMN binding site from MD simulations. The value of each volume element (voxel) corresponds to the average number of water oxygens occupying it; the voxels span 0.5 Å along each dimension and are arranged in a grid along arbitrary orthogonal axes. The median value for bulk water was found to be 0.475 water/voxel; blue, green, and red isosurfaces indicate occupancies of 1 ×, 0.5 ×, and 0.25 × the density of bulk water, respectively. Clockwise from top left, occupancies averaged over simulations D_WT1−5, L_WT1−5, L_F434Y1−3, and D_F434Y1−3.

maps of the water occupancies observed in both the wild-type and F434Y mutant simulations are compared in Figure 3. Among all four states (i.e., F434Y and wild type under both light and dark conditions), a total of three different major water binding sites are resolved: (1) one adjacent to Asn492 and distal to FMN, between the Iβ strand and Cα helix (which will be termed the antechamber site), (2) one positioned to interact with the O4 atom of FMN, a similar site interacting with the FMN N5 atom, and (3) one adjacent to Cys450 distal to FMN as observed in the crystal structure.[29] Site 1 corresponds to a previously identified void in several LOV domain crystal structures proposed to allow imidazole occupancy near the chromophore (site 2 of ref 41), but the others have not been identified previously and appear to emerge only in some noncrystallographic conformations sampled during MD simulations. The occupancies of these three sites throughout the simulations reported here, and their correlations with the conformation of Q513, are listed in Tables SI1 and SI2 of the Supporting Information. Very little water binding in the sites interacting directly with FMN is apparent in the wild-type dark-state simulations, and when present, such water molecules do not cause Q513 to lose contact with O4. However, the photo-adduct state allows water to bind to both the O4 and N5 sites, displacing Gln513 as discussed above; as seen in Tables SI1 and SI2 of the Supporting Information, the occupancy of conformations in which Gln513 can form a hydrogen bond with the O4 atom of FMN drops from 0.7 to 0.25 from the dark state to the light state.[33]

As expected, the F434Y mutation significantly alters the pattern of water binding in the vicinity of FMN (Scheme 1); in the F434Y dark state, strong occupancy of the N5 site is observed, although the location of water binding is slightly above the FMN plane (vs in the plane in the wild-type light state). This occurs because the water molecules bound here are generally hydrogen bonded with both Tyr434 and FMN. The F434Y light state shows a stronger water occupancy of the O4 site and a weaker occupancy of the N5 site but is otherwise similar to the wild-type light state. These water binding sites strongly influence the behavior of Gln513, as displacement of Gln513 from FMN occurs primarily in the presence of water molecules bound to the O4 and N5 sites. When in the flipped conformation, Gln513 can interact with both the water that displaces it and the antechamber water.

As observed in the crystal structures of CrLOV1 (*Chlamydomonas reinhardtii* phototropin 1 LOV1)[37] and AsLOV2,[29] the MD simulations of wild-type AsLOV2 resolved two conformations of Cys450, differing by rotation about the χ_1 angle (Figure 2C,D). Similar cysteine inhomogeneity can be observed in FTIR measurements.[42,43] In conformation I, Cys450 is rotated to a position with its sulfur atom directly above the C4a atom of FMN, whereas in conformation II, the cysteine is rotated from the C4a atom and toward a water binding site. The occupancies of conformations I and II extracted from the CrLOV1 and AsLOV2 crystal structures are strongly biased toward conformation II (0.3:0.7 for CrLOV1[37] and 0.1:0.9 for AsLOV2).[29] However, our MD simulations of wild-type AsLOV2 in solution yield

Table 1. Kinetic Rate Constants in the Description of WT and F434Y Conformer Exchange

		wild type (A)	F434Y (B)
MD simulation conformer rate constants[a]	$k_{I \rightarrow II}$	$(2400 \text{ ps})^{-1}$	$(950 \text{ ps})^{-1}$
	$k_{II \rightarrow I}$	$(900 \text{ ps})^{-1}$	$(2400 \text{ ps})^{-1}$
MD simulation conformer occupancies	conformer I	74.5%	28.8%
	conformer II	25.5%	71.1%
conformer rate constants	$k_{I \rightarrow II}$	$(1200 \text{ ps})^{-1}$	$(1100 \text{ ps})^{-1}$
	$k_{II \rightarrow I}$	$(900 \text{ ps})^{-1}$	$(1875 \text{ ps})^{-1}$
conformer occupancies	conformer I	57%	37%
	conformer II	43%	63%
$S_2 \rightarrow S_1$ rate constants	$^{I}k_{vib,IC}$	$(1 \text{ ps})^{-1}$	$(0.3 \text{ ps})^{-1}$
	$^{II}k_{vib,IC}$	$(0.5 \text{ ps})^{-1}$	$(0.3 \text{ ps})^{-1}$
radiative rate constants	$^{I}k_{rad}$	$(17 \text{ ns})^{-1}$	$(17 \text{ ns})^{-1}$
	$^{II}k_{rad}$	$(17 \text{ ns})^{-1}$	$(17 \text{ ns})^{-1}$
IC rate constants	$^{I}k_{IC}$	$(20 \text{ ns})^{-1}$	$(1.68 \text{ ns})^{-1}$
	$^{II}k_{IC}$	$(21 \text{ ns})^{-1}$	$(2.15 \text{ ns})^{-1}$
ISC rate constants	$^{I}k_{ISC}$	$(1.5 \text{ ns})^{-1}$	$(1.5 \text{ ns})^{-1}$
	$^{II}k_{ISC}$	$(3.0 \text{ ns})^{-1}$	$(3.0 \text{ ns})^{-1}$
triplet quantum yield, ϕ	$\phi_{I,ISC}$	87%	41%
S–FMN distances	conformer I S–FMN mean distance	3.74 Å	3.80 Å
	conformer II S–FMN mean distance	4.54 Å	4.84 Å

[a] Estimated conformer equilibration rate constants are underestimated by 30–90% because of the use of a Langevin thermostat.

different occupancies of 0.74 ± 0.03 and 0.25 ± 0.03 for the conformation I and II states, respectively (treating each nonoverlapping 50 ns segment of the trajectory as a statistically independent measurement). The F434Y mutation significantly alters the energetics and kinetics of Cys450 rotation to favor conformer II with occupancies of 0.29 ± 0.05 and 0.71 ± 0.05 for conformers I and II, respectively (Table 1).

The MD simulations described above demonstrate that interconversion between C450 conformers is rapid, occurring on nanosecond time scales in both the wild-type and F434Y structures. The distribution of dwell times in one conformation prior to switching in the wild-type dark state can be fitted with a single-exponential decay with rate constants of $(2400 \text{ ps})^{-1}$ and $(890 \text{ ps})^{-1}$ for the I → II and II → I transitions, respectively. Coincidentally, the rates for the same transitions in the F434Y dark state are almost exactly reversed, $(950 \text{ ps})^{-1}$ and $(2400 \text{ ps})^{-1}$ for the I → II and II → I transitions, respectively. Introducing the F434Y mutation shifts the free energy difference between the rotamers by ~1 kcal/mol to more strongly favor conformation II, presumably because of steric hindrance by the Tyr434 phenolic oxygen and the introduction of a water binding site that competes with conformer I. Because of the formation of a covalent bond between Cys450 and the C4a atom of FMN, conformation II is not populated in any of the light-state simulations.

Structural Effects of the F434Y Mutation as Identified by Solution NMR. To establish the effects of the F434Y point mutation on the AsLOV2 structure, we compared multidimensional NMR spectra acquired on uniformly ^{15}N-labeled samples of the wild-type and F434Y forms of the protein. An overlay of two-dimensional ^{15}N–^{1}H HSQC spectra of both proteins (Figure SI2a of the Supporting Information) shows similar overall patterns of cross-peaks, with only a subset of sites being affected. This is qualitatively consistent with only minor perturbations of the overall LOV domain structure. More detailed analysis using the minimal chemical shift difference method,[44] which conservatively estimates changes between a fully assigned reference protein (i.e., wild-type

AsLOV2) and the unassigned mutant, shows that structural effects are primarily focused to the region around the F434Y point mutation (Figure SI2b,c of the Supporting Information). Several sites near the FMN chromophore are affected, but a limited number of locations overall are perturbed. Taken together, these data are consistent with the F434Y protein maintaining a global structure similar to that of the wild-type protein, with minor conformational changes near Tyr434, Cys450, and the isoalloxazine ring.

Ultrafast Triplet Formation Dynamics (<10 ns). The static absorption spectra of both wild-type AsLOV2 and the F434Y mutant are very similar (Figure 4A), with vibronic peaks at 422, 447, and 474 nm associated with the $S_0 \rightarrow S_1$ transition. A higher-energy $S_0 \rightarrow S_2$ transition overlaps the $S_0 \rightarrow S_1$ transition and peaks near 365 nm.[45] The measured femtosecond to microsecond photodynamics for both systems were initiated via 400 nm ultrafast excitation. Although this introduces excess vibrational energy into the system versus lower energy excitation, it has previously been established that excitation wavelengths between 360 and 470 nm produce similar photocycles and quantum yields.[46,47]

The subnanosecond photoinduced signals in F434Y and the wild type exhibit similar spectroscopic features (Figure 4B,C). Immediately upon 400 nm photoexcitation, a negative ground-state bleach (GSB) between 400 and 500 nm is observed, concomitant with a negative stimulated emission (SE) band near 540 nm and positive excited-state absorption (ESA) bands at 510 and >625 nm. Because the transient spectra in Figure 4 resolve both the bleach and excited-state signals simultaneously, a complete model with ground-state recovery kinetics can be constructed. In the F434Y sample, the subpicosecond signals exhibit a fast (~2 ps) blue shift of the SE band that is ascribed to vibrational cooling of the S_1 population (Figure 4C).[48] Transient signals induced with lower-energy excitation (470 nm) do not exhibit this subpicosecond behavior.[27,41] The 1 ps spectrum is similar to the excited singlet spectrum previously identified for
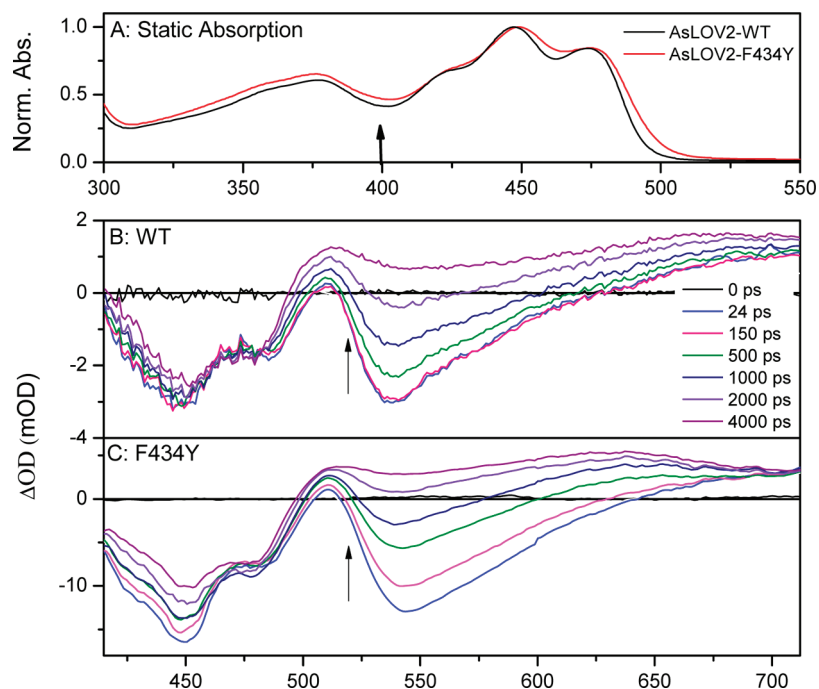
Figure 4. (A) Normalized absorption spectra of wild-type AsLOV2 (black lines) and the F434Y mutant (red line), in 50 mM sodium phosphate buffer (pH 6.0) with 100 mM NaCl. The arrow indicates the excitation wavelength for the transient experiments. Ultrafast transient absorbance spectra of (B) wild type and (C) F434Y. Arrows denote the transient trend of data as the singlet S_1 population evolves to the triplet population. Note that the F434Y mutant exhibits greater transient loss of bleach (<500 nm) signal than the wild-type signals.

oxidized FMN,[48] and the 7 ns spectrum strongly resembles the known triplet-state spectrum of flavin with a broad absorption band extending from 490 nm into the red.[49] Apart from this fast vibrational relaxation, the observed dynamics agree well with previous ultrafast measurements on wild-type AsLOV2 by Kennis and co-workers[27] with the initial photoexcited singlet state generating an excited triplet state on a nanosecond time scale. The addition of imidazole, used to accelerate the ground-state recovery kinetics, does not affect the ultrafast ISC kinetics in either sample (data not shown).[31,32,41]

The differences between wild-type AsLOV2 and F434Y signals are more apparent when viewed temporally and differ in both time scale and functional form (Figure 5 and Figure SI3 of the Supporting Information). The singlet excited state (with its characteristic SE and ESA bands) decays distinctly faster for F434Y than for wild-type AsLOV2. Global multiwavelength fits to the wild-type AsLOV2 data demonstrate that a single-exponential decay with a τ of 2.09 ns (Figure SI3 of the Supporting Information) is sufficient to describe the data well, in agreement with previous measurements of Kennis and co-workers.[27] In contrast, the F434Y mutant photodynamics required a biexponential decay model with time constants of 320 ps (34%) and 1.4 ns (66%) to describe the data (Figure SI3B of the Supporting Information).

Adduct Formation Dynamics (10 ns to 5 μs). Although the triplet-state formation kinetics is clearly resolved in the sub-10 ns signals, the subsequent decay and adduct formation dynamics between Cys450 and FMN evolve on a microsecond time scale that cannot be directly monitored with the ultrafast apparatus. To characterize the adduct formation dynamics that quench the triplet population, the time-resolved signals of the triplet state were probed at 640 nm, near the peak of the triplet absorption
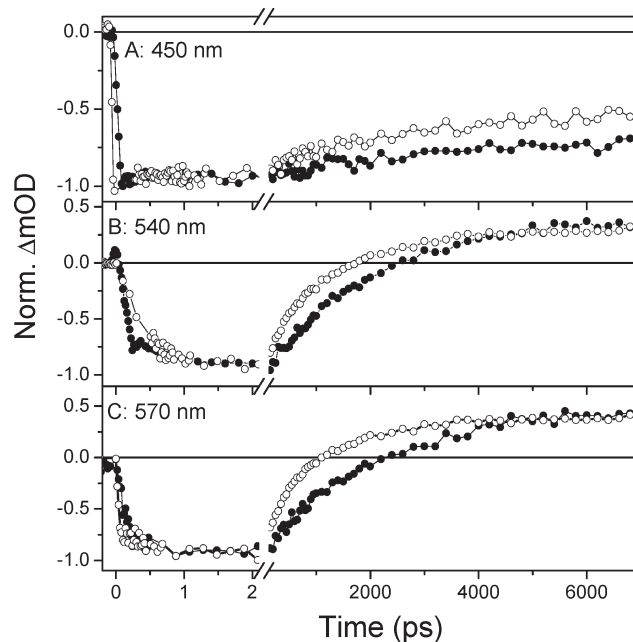

Figure 5. Ultrafast transient absorption kinetic traces probed at select wavelengths (λ_{pr}) of wild-type AsLOV2 (●) and F434Y (○) during the formation of the triplet state via intersystem crossing. λ_{pr} = 450 (A), 540 (B), and 570 nm (C).

spectrum (Figure 4B,C). The adduct absorbs very weakly at this wavelength.[19] The parameters extracted from fitting these data to a sum of exponentials are comparable (Table SI4 of the Supporting Information) to those of other LOV studies.[31] The triplet-state decay for the wild-type protein can be fit with a
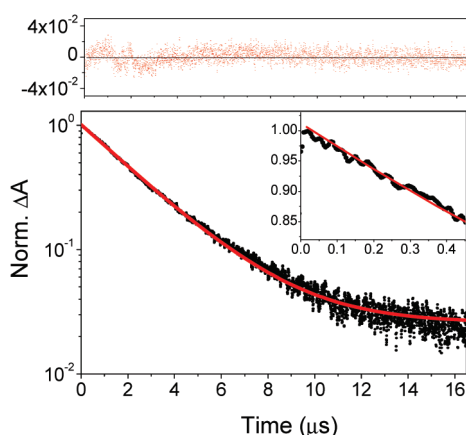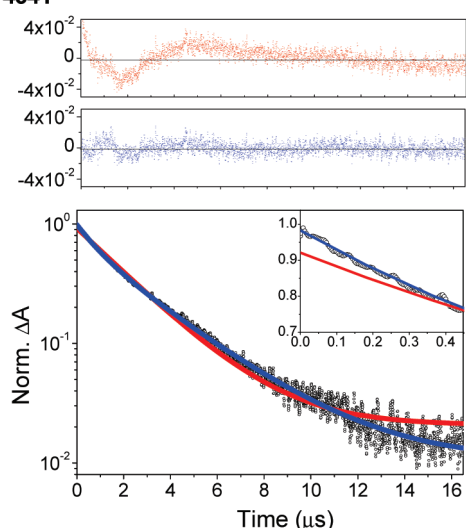
A: wildtype AsLOV2

B: F434Y

Figure 6. Triplet-state decay kinetics of wild-type AsLOV2 (A) and F434Y (B) at 640 nm near the peak of triplet-state absorption (Figure 4B,C). Excitation pulses were centered at 400 nm with an energy of 160 nJ. Experimental data (circles) were normalized at the peak signal (time zero). Red lines indicate a single-exponential fit, whereas blue lines show a biexponential fit. Data and fits at early times are compared in insets. Residuals of fits are contrasted in the top panels as indicated. The transient data were best fit with the following functions: $A(t) = 0.98e^{-t/2.50} + 0.025$ and $A(t) = 0.33e^{-t/0.93} + 0.64e^{-t/3.02} + 0.010$ for the wild type and F434Y, respectively, with t in units of microseconds. The small (1%) static amplitude represents the weak absorption of the adduct photoproduct.

single-exponential decay with a 2.49 μs time constant (Figure 6A). In contrast, the F434Y signals require a biexponential model to achieve a comparable quality of fit (Figure 6B), with time constants of 3.02 μs (66%) and 0.93 μs (34%). As with the ultrafast triplet formation kinetics, the addition of imidazole to either sample does not affect the observed triplet decay kinetics (data not shown).

Adduct Decay Dynamics (500 ms to 100 s). The photoadduct recovery kinetics in wild-type AsLOV2 exhibits a monoexponential decay with a time constant of 85 s under the conditions used for the protein sample. Although this time scale is longer than that previously observed for AsLOV2 (e.g., 45 s observed in ref 40), different sample conditions were used here. The F434Y mutant also exhibits monoexponential photoadduct

recovery kinetics, but with an appreciably faster time constant of 7.8 s [at 25 °C in pH 6.0 buffer (see Figure SI7 of the Supporting Information)]. The F434Y mutation also induced a greater sensitivity (observed as an acceleration) of the adduct decay kinetics to residual imidazole in the buffer than for the wild type (data not shown), indicative of the greater solvent access to the FMN cofactor for the F434Y mutant identified in the MD simulations.

■ DISCUSSION

Intersystem Crossing Dynamics (100 fs to 10 ns). The ultrafast kinetics of the studied LOV domains shown in Figures 4 and 5 are strongly dominated by the high-yield (>50%) ISC dynamics that generate the reactive triplet populations. For wild-type AsLOV2, these signals can be described well with a single-2 ns exponential model in agreement with Kennis and co-workers.[27] In contrast, fitting the F434Y signals requires multiple exponential components (Figure SI3 of the Supporting Information), which is often interpreted as a signature of an underlying inhomogeneity. The coexistence of two conformations of Cys450 offers a convenient and often-used justification for the multiexponential microsecond kinetics in LOV domains. For wild-type AsLOV2, the occupancies of conformations I and II in the X-ray crystal structures are estimated to be 10 and 90%, respectively.[29] The MD simulations of wild-type AsLOV2 demonstrate that the two conformations are in a dynamic equilibrium with Cys450 flipping from one conformer to the other on a nanosecond time scale.[33,42] A static phenomenological model consisting of two separate populations exhibiting differing ISC kinetics can be constructed to characterize the F434Y signals (Figure SI4C of the Supporting Information). This model, however, does not sufficiently explain both the biexponential kinetics of the F434Y mutant and the monoexponential kinetics in wild-type AsLOV2,[27] given that the MD simulations demonstrate that interconformation population flow occurs on time scales comparable to those of the ISC dynamics for both wild-type and F434Y AsLOV2.

Rather, the underlying ultrafast signals for both proteins require a dynamic multistate model that incorporates the interchange of conformers identified in the MD simulations. Underlying this "dynamic conformer model" in Figure 7 is the fact that both cysteine conformations differ not only in orientation but also in the average distance between the sulfur atom of Cys450 and the FMN cofactor (Table 1). From the MD simulations, these distances are on average 3.80 Å (conformer I) and 4.84 Å (conformer II) for F434Y and 3.74 Å (conformer I) and 4.54 Å (conformer II) for wild-type LOV2. It is known that the addition of sulfur atoms to riboflavin solutions in DMSO enhances ISC kinetics[50] and that Cys → Ser mutations that remove the sulfur atom of the conserved cysteine residue in CrLOV1 (Cys57 in CrLOV1 and Cys450 in AsLOV2) significantly slow ISC dynamics (from $\tau_F = 2.9$ ns to $\tau_F = 4.6$ ns).[50,51] The heavy atom mechanism affecting ISC dynamics is a spin−orbit coupling that scales exponentially with the distance between the sulfur and the FMN chromophore.[52−54] The ISC rates are thus strongly modulated by the conformer occupations and the underlying Cys450 flipping dynamics.[55,56]

The dynamic conformer model in Figure 7 separates the photodynamics into contributions from the two conformers with different intrinsic ISC rates, with population flow occurring between them. Although more complicated than a static
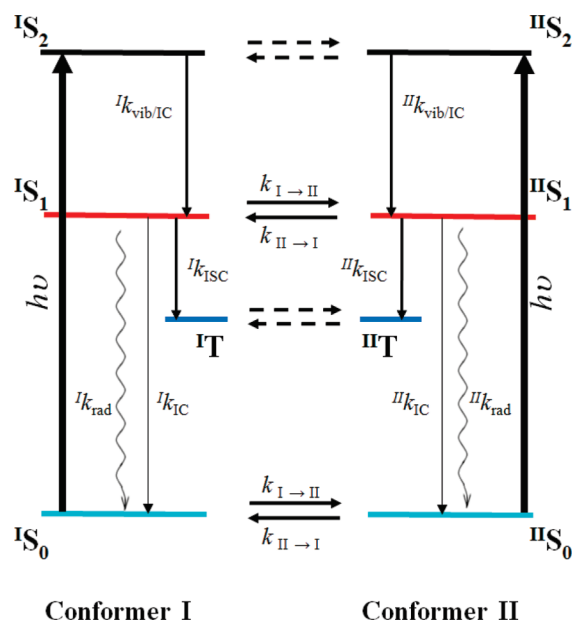
Figure 7. Dynamic conformer model used to fit both wild-type and F434Y mutant ultrafast dynamics. The connectivity consists of two photoexcited populations (conformer I and conformer II) representing different conformer states (and distances to the FMN chromophore) of the Cys450 residue. Each population is indicated via right superscripts; 400 nm photoexcitation pulses (thick vertical black lines) excite both the S_2 and higher-lying vibrationally excited S_1 (black lines) in each conformer population. Evolution via vibrational relaxation and S_2 to S_1 occurs via internal conversion. The S_1 population persists for nanoseconds and decays via either intersystem crossing to the triplet state (blue line), radiative emission (wavy lines), or internal conversion to the ground-state populations (cyan curve). Horizontal lines represent interconformer dynamics. The modeling explicitly included the interconformer conversion of the S_0 and S_1 populations (which were locked to the same kinetics); the dashed lines presumably exist but do not affect the signals and were ignored for the sake of convenience. Initial occupations of each conformer population result exclusively from the interconformer time constants. States are color-coded to spectra and concentration profiles in Figure SI6 of the Supporting Information.

inhomogeneous model (Figure SI4C of the Supporting Information), a number of constraints can be introduced to limit the range of estimated parameters to describe the transient data. (1) The species-associated difference spectrum (SADS)[57,58] that describes the spectrum for each contributing population in the dynamics is assumed to be insensitive to the C450 conformation ($^IS_1 = \ ^{II}S_1$). (2) The initial occupancies of the conformers are determined exclusively by the isomerization time constants, where the occupancy ratio is equal to the ratio of isomerization time constants. (3) The ISC time constants for each conformer flow are independent of the sample (i.e., $^Ik_{ISC}$ for wild-type AsLOV2 is the same as $^Ik_{ISC}$ for the F434Y mutant). (4) The radiative, ISC, and internal conversion (k_{IC}) time constants are accurately described by simultaneously fitting the ground-state bleach recovery and the excited-state signal. (5) Reasonable agreement with MD simulations of conformer time constants, including both time scales and trends, is found.

Subject to the constraints described above, the dynamic conformer model accurately describes both wild-type AsLOV2 and the F434Y mutant ultrafast signals (Figure 8) with the parameters outlined in Table 1. The concentration profiles for the contributing populations and their SADS are compared in

Figure SI6 of the Supporting Information.[57,58] Although intrinsically multiexponential in decay character, the predicted dynamics for the wild-type AsLOV2 sample is primarily monoexponential because of the trade-off of occupancies and intrinsic ISC time scales described below. In agreement with the MD simulations, the combination of the greater conformer I occupancy (57%) versus that of conformer II (43%) with the faster interconformer kinetics of conformer II to conformer I (900 ps) versus the reverse (1200 ps) generates nearly monoexponential behavior. In contrast, the F434Y mutation alters the conformer occupancies to favor conformer II (37% vs 63%), with a slower interconformer time scale (conformer I to conformer II), which generates biexponential ISC kinetics.

While the time constant for rotation of Cys450 from conformation II to conformation I in MD simulations is approximately 2.5-fold too slow ($k_{I\rightarrow II}^{-1} = 2400$ ps, and $k_{II\rightarrow I}^{-1} = 900$ ps) to match the experimentally observed slow component of the F434Y ISC kinetics (2400 ps), the Langevin thermostat in the MD simulations is known to underestimate true rates of barrier crossing.[59] Indeed, in 200 ns simulations of both the wild-type and F434Y dark states in the NVE ensemble (i.e., with no thermostat), all Cys450 rotation rates except for the wild-type $k_{I\rightarrow II}$ were estimated to be faster, by factors of $1.3-1.9$ (data not shown). This accounts for the small discrepancy with experimental time scales used in the global modeling and the MD simulations.

As indicated by the bleach recovery dynamics in Figure 5A, the F434Y mutation also induces faster IC population kinetics. This may originate from the presence of the water molecule identified in the MD simulations (Figure 2) that can hydrogen bond to the FMN to facilitate a faster quenching mechanism.[60] The peak of the static absorption spectrum of F434Y is red-shifted compared to that of the wild type (Figure 4A). This spectral shift may reflect a local reordering of hydrogen bonding around the FMN with the hydroxyl group of the newly introduced tyrosine forming a new hydrogen bond to some amino residue in the AsLOV2 domain (Scheme 1).[61] It has been observed that the lack of hydrogen bonding between *A. capillus-veneris* phy3 LOV2-Q1029L and FMN induces a similar blue-shifted absorption spectrum in the dark.[36] The molecular dynamics simulations suggest that Tyr434 accepts a new hydrogen bond to a water molecule (Figure 3), which mediates interactions between Cys450 and the O4 atom of FMN. Even though the ISC rate constants are distinctly faster for the F434Y mutant, which increases the triplet yield and overall photosensitive efficiency of the protein, an increase in IC time scales, which reduces the triplet yield, counters this increase perfectly to generate a nearly identical yield for both wild-type and F434Y proteins. An alternative mechanism underlying this faster IC for the F434Y mutant involves a competing electron transfer process from the introduced tyrosine to FMN that would quench the singlet excited state. A similar mechanism has been proposed for activating BLUF domains[46,62] whereby a conserved Tyr donates an electron to the photoexcited flavin. However, the transient data do not support the growth of a secondary reduced quinoid species overlapping the singlet and triplet populations, which indicates that if an electron transfer mechanism were at work in the LOV2 domains, it would not result in stable intermediates as the latter would rapidly recombine to recover the ground state.

Adduct Formation Dynamics (100 ns to 5 μs). Many naturally occurring LOV domains (e.g., AsLOV2 and *Bacillus subtilis* YtvA LOV) exhibit single-exponential microsecond
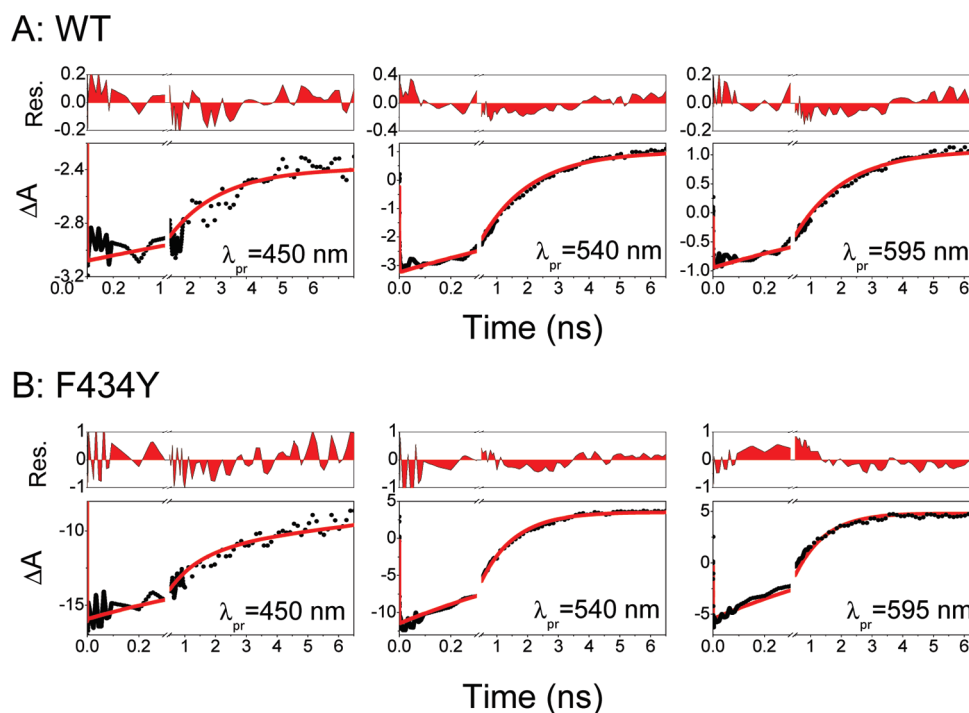
Figure 8. Decay kinetic traces of wild-type AsLOV2 (A) and F434Y (B) ultrafast signals detected at different probe wavelengths λ_{pr}. Solid lines indicate fits obtained from the dynamic inhomogeneous model outlined in Figure 7. Interconformer kinetics parameters were obtained via MD simulations. The S_2, S_1, and T populations for each conformer were locked to each other as were the same intersystem crossing time constants for each conformer in both samples (Table 1). Releasing these temporal constraints results in slightly better fits (Supporting Information) but leads to the loss of information regarding the connectivity between the C450 isomerization dynamics and observed ISC dynamics observed in both samples. Residuals are shown in the top panels.

photoadduct formation kinetics, whereas others (e.g., CrLOV1) exhibit biexponential kinetics (Table SI3 of the Supporting Information). The single-exponential decay kinetics of the wild-type AsLOV2 triplet state (Figure 6A) suggests that either a single photoadduct population exists or an inhomogeneity is "equilibrated out" on a faster time scale to generate an effective homogeneous system with a rapid population flow between the two populations (e.g., conformers). The F434Y mutation of AsLOV2 switches the protein from exhibiting single- to double-exponential triplet decay kinetics, with one phase approximately 2.5 times faster ($0.93 \mu s$) and a second phase slightly slower ($3.02 \mu s$) than that of wild-type AsLOV2. The nature of the inhomogeneity responsible for the biexponential triplet decay kinetics in the F434Y mutant is not resolved in the data presented here and is outside the time scales of MD simulations. Because the dynamic equilibration of the Cys450 that manipulates the ISC kinetics on the nanosecond time scale will "average out" on the slower microsecond time scale, the contributions of various local interactions to the FMN cofactor such as hydrogen bonding and van der Waals interactions on the cysteinyl−FMN adduct formation kinetics must be considered. The fast kinetic phase could arise either because the introduced Tyr434 residue alters the conformational distributions of the flavin and Cys450 (Scheme 1) to accelerate adduct formation or because Tyr434 (or the binding site water bound adjacent to it) directly participates in adduct formation (e.g., by acting as an acid−base catalyst to deprotonate Cys450 and protonate N5 of the flavin). Because the dark-state MD simulations show that water binding and unbinding in the FMN pocket occur on time scales of tens of nanoseconds, which is orders of magnitude too fast to explain the multiple kinetic phases observed on a microsecond time scale, this eliminates the

presence or absence of water as the cause of the two kinetic phases in the mutant signals unless the exchange of water into the binding site is radically slower in the triplet state (not simulated).

It is more likely that a slow, large-scale structural change exists in the F434Y mutant that gives rise to a configuration (e.g., because of the relative orientation of Tyr434 and the flavin) that more rapidly forms the photoadduct. Chemical shift NMR analysis (Figure SI2 of the Supporting Information) indicates that in the F434Y mutant, sites near Tyr434, Cys450, and the O1, N2, O3 portion of the isoalloxazine ring undergo small changes while the rest of the protein remains the same as the wild type.

Adduct Decay Dynamics (500 ms to 100 s). On the basis of observations that the I427V mutation accelerates adduct decay kinetics by destabilizing the adduct through the removal of favorable contacts,[31] free energy perturbation (FEP) calculations were performed (Supporting Information) to quantify the change in photoadduct stability for the F434Y mutant compared to the wild-type protein. Energetic destabilization of the photoadduct in the F434Y mutant is unlikely to be a factor for the rapid recovery time scale, as FEP calculations indicate that the photoadduct is more stable in the F434Y mutant than in the wild type, by 1.0 ± 0.3 kcal/mol (with error bars based on block averaging of 10 blocks and given at two standard deviations). The molecular nature of the increased adduct stability for F434Y is unresolved, but the removed constraints of the unfolded Jα helix force a structural perturbation in the Iβ strand to induce a small movement of Tyr434 on the Cα helix through flipping of Gln513 and Asp517. The water molecule that donates the new hydrogen bond to Tyr434 (Scheme 1) shifts the conformation properties of Cys450, and this structural change in F434Y alters the dihedral distribution of Cys450 and the conformation of Gln513.[33]
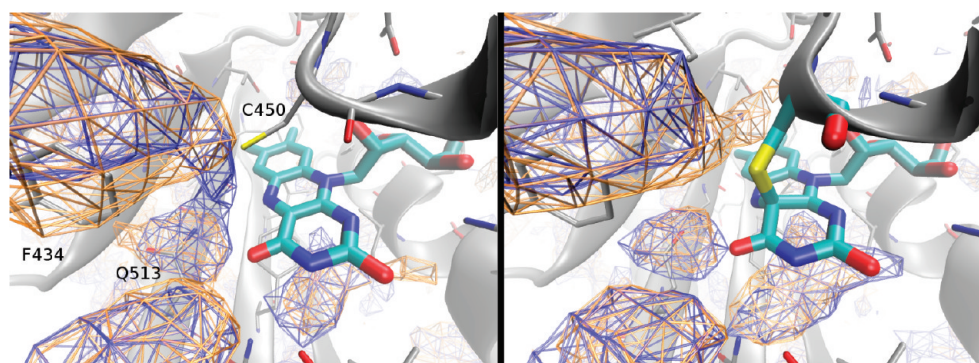
Figure 9. Oxygen accessibility of AsLOV2 from MD simulations, calculated using implicit ligand sampling. The left panel shows the dark-state oxygen accessibility for wild-type (blue) and F434Y (orange) AsLOV2. An isosurface is shown at a free energy change equivalent to that for moving oxygen from vacuum into bulk TIP3 water (1.97 kcal/mol).[64] The right panel shows the light-state oxygen accessibility for wild-type (blue) and F434Y (orange) AsLOV2. Isosurfaces are defined as for the left panel.

The resulting changes in the C4a-distal rotamer and water occupancy for two different conformers might induce β-strand loosening, resulting in faster adduct formation in the light-adapted state and faster adduct relaxation in the dark state (Figure 6 and Figure SI7 of the Supporting Information).

To test alternative causes of the accelerated photoadduct decay in the F434Y mutant, we explored the solvent (Figure 3) and oxygen (Figure 9) accessibility of the binding site. Implicit ligand sampling calculations[64] based on the equilibrium MD trajectories indicate the presence of an expanded oxygen-accessible region immediately adjacent to the cysteinyl—flavin bond in the F434Y photoadduct. The estimated free energy for oxygen binding in this region is approximately 2.5 kT more favorable for F434Y than for the wild-type protein. The obtained solvent accessibility maps (Figure 3) indicate a significantly enhanced water binding site adjacent to the O4 atom of the light-adapted photoadduct in the F434Y mutant. This raises the possibility of a water-catalyzed decay mechanism (the same site is also presumably responsible for the enhanced imidazole sensitivity of the F434Y mutant) for recovery dynamics, which is, in part, supported by D_2O/H_2O kinetic isotope effects observed in the recovery of wild-type AsLOV2 by Bogomolni and co-workers that identifies a proton transfer reaction involved in initiating recovery dynamics.[19,63] Both the oxygen and water accessibility analyses was performed on trajectories that began, and remained, in the Jα-associated conformation, because of the very long (by MD standards) time scales for Jα dissociation. Hence, the water and oxygen accessibility may thus be further altered by the dissociation of Jα, in the light state. In biased MD simulations in which Jα was completely dissociated from the β sheet core, no substantial changes to the FMN binding site were observed besides rotation of Q513 as noted above (P. Freddolino, unpublished data), suggesting that the nondissociated simulations provide a good approximation for the vicinity of the FMN binding site in the Jα-dissociated, light-adapted state.

To evaluate the hypothesis that the increased accessibility of molecular oxygen to the FMN binding pocket in the F434Y mutant is, at least in part, responsible for the accelerated recovery time scale of the mutant versus the wild type, we measured the recovery kinetics in samples exposed to oxygen in the air contrasted with samples purged with argon (Figure SI8 of the Supporting Information). A clear deceleration of the recovery time scales is observed in the purged, but freshly exposed to air, sample versus the fully exposed samples. Furthermore, when the

argon-purged sample is exposed to air for more than 5 min, kinetics nearly identical to that of the nonpurged sample can be observed, indicative of the sensitivity of O_2 to the recovery mechanism. In agreement with our MD simulations, the recovery kinetics of wild-type samples exhibits a significantly weaker sensitivity to oxygen (not shown) because of a lower level of exposure of the cysteinyl—FMN adduct to O_2.

Clearly, exposure to molecular oxygen facilitates adduct disruption and results in an oxidation of the FMN to re-form the dark-adapted population. Although molecular oxygen is known to break thioether bonds to generate oxidized sulfoxide species,[65,66] no persistent degradation of the F434Y mutant was observed in our measurements. This suggests that O_2 catalyzes the adduct bond breakage but does not incorporate directly into the FMN or the cysteine residue, which would essentially inactivate the protein photoactivity. Alternatively, the isoalloxazine ring of the FMN is established as an excellent electron acceptor capable of many interesting redox chemistries, which can involve one to two electron oxidation processes.[67] Flavins can form transient adducts with molecular oxygen observed in many flavin-dependent flavoenzymes,[68,69] including oxidases and dehydrogenases. These new peroxy adducts may potentially displace the FMN—S bond but also result in the incorporation of oxygen atoms into substrate species (e.g., cysteine in AsLOV2) like the chemistry of direct attack of the thioether bonds. The exact mechanism underlying the observed oxygen-catalyzed adduct breakage in F434Y is unclear and is a topic of further study. It should also be noted that although the purging of O_2 significantly slows the recovery kinetics, the observed time scales in purged F434Y samples are still considerably faster than those observed in wild-type AsLOV2 (Figure SI7 of the Supporting Information), so other unresolved factors (e.g., acid/base catalysis by Y434) must also contribute to the faster photocycle recovery.

■ CONCLUDING COMMENTS

LOV domains are of particular interest at present for their suitability for basic science and engineering applications, many of which are based on approaches to conferring photosensitivity to target proteins via genetic fusion of LOV domains onto exogenous targets.[5] While LOV domains have several natural advantages compared to other sensory domains for such engineering, including their small size and use of common FMN and FAD chromophores, certain properties may not always be ideal for any

one application. Versions of AsLOV2 and other LOV domains containing point mutations that confer "improved" characteristics (e.g., dynamic range)[70] can therefore be valuable as both research reagents and vehicles for testing mechanistic hypotheses. Unfortunately, identifying new mutations with beneficial properties is challenging; rational design is slow, and genetic selection strategies are highly dependent on assay conditions for identification of a novel phenotype. Our work demonstrates the merits of a combined computational—experimental approach to identifying a novel mutant in a residue outside the chromophore-binding pocket to generate an AsLOV2 variant with new photochemical properties. Future use of such an approach, perhaps accelerated through the use of coarse-grained computational and rapid experimental methods, will be essential for identifying additional mutations useful for biophysical study and applications.

■ ASSOCIATED CONTENT

Ⓢ Supporting Information. Details of (1) sample expression and purification, (2) MD simulation methods, (3) MD simulations of GLN513 dynamics, (4) solution NMR signals, (5) chemical shift difference maps, (6) time-resolved methods, (7) global analysis details underlying dispersed transient data, and (8) adduct recovery signals. This material is available free of charge via the Internet at http://pubs.acs.org.

■ AUTHOR INFORMATION

Corresponding Author
*E-mail: dlarsen@ucdavis.edu. Phone: (530) 754-9075. Fax: (530) 752-8995.

Present Addresses
‖Lewis-Sigler Institute for Integrative Genomics, Princeton University, Washington Road, Princeton, NJ 08544.

■ ACKNOWLEDGMENT

■ ABBREVIATIONS

LOV, light, oxygen, and voltage sensitive; AsLOV2, second LOV domain of *A. sativa* phototropin 1; BLUF, blue light sensors utilizing flavin; FAD, flavin adenine dinucleotide; FMN, flavin mononucleotide; PYP, photoactive yellow protein; ISC, intersystem crossing; MD, molecular dynamics; CrLOV1, *C. reinhardtii* light, oxygen, and voltage domain 1; GSB, ground-state bleach; SE, stimulated emission; ESA, excited-state absorption; SADS, species-associated difference spectrum; FEP, free energy perturbation.

■ REFERENCES

(1) Briggs, W. R., and Spudich, J. L. (2005) *Handbook of Photosensory Receptors*, Wiley-VCH Verlag GmbH & Co. KGaA, Weinheim, Germany.

(2) Hoersch, D., Otto, H., Cusanovich, M. A., and Heyn, M. P. (2009) Time-resolved spectroscopy of dye-labeled photoactive yellow protein suggests a pathway of light-induced structural changes in the N-terminal cap. *Phys. Chem. Chem. Phys. 11*, 5437–5444.

(3) Moglich, A., Ayers, R. A., and Moffat, K. (2009) Structure and signaling mechanism of Per-ARNT-Sim domains. *Structure 17*, 1282–1294.

(4) Moglich, A., Yang, X., Ayers, R. A., and Moffat, K. (2010) Structure and function of plant photoreceptors. *Annu. Rev. Plant Biol. 61*, 21–47.

(5) Zoltowski, B. D., and Gardner, K. H. (2011) Tripping the Light Fantastic: Blue-Light Photoreceptors as Examples of Environmentally Modulated Protein-Protein Interactions. *Biochemistry 50*, 4–16.

(6) van der Horst, M. A., and Hellingwerf, K. J. (2004) Photoreceptor proteins, "star actors of modern times": A review of the functional dynamics in the structure of representative members of six different photoreceptor families. *Acc. Chem. Res. 37*, 13–20.

(7) Losi, A. (2007) Flavin-based Blue-Light photosensors: A photobiophysics update. *Photochem. Photobiol. 83*, 1283–1300.

(8) Rockwell, N. C., Su, Y. S., and Lagarias, J. C. (2006) Phytochrome structure and signaling mechanisms. *Annu. Rev. Plant Biol. 57*, 837–858.

(9) Masuda, S., and Bauer, C. E. (2002) AppA is a blue light photoreceptor that antirepresses photosynthesis gene expression in *Rhodobacter sphaeroides. Cell 110*, 613–623.

(10) Lin, C., Robertson, D. E., Ahmad, M., Raibekas, A. A., Jorns, M. S., Dutton, P. L., and Cashmore, A. R. (1995) Association of flavin adenine dinucleotide with the *Arabidopsis* blue light receptor CRY1. *Science 269*, 968–970.

(11) Huala, E., Oeller, P. W., Liscum, E., Han, I. S., Larsen, E., and Briggs, W. R. (1997) *Arabidopsis* NPH1: A protein kinase with a putative redox-sensing domain. *Science 278*, 2120–2123.

(12) Christie, J. M., Salomon, M., Nozue, K., Wada, M., and Briggs, W. R. (1999) LOV (light, oxygen, or voltage) domains of the blue-light photoreceptor phototropin (nph1): Binding sites for the chromophore flavin mononucleotide. *Proc. Natl. Acad. Sci. U.S.A. 96*, 8779–8783.

(13) Briggs, W. R., and Christie, J. M. (2002) Phototropins 1 and 2: Versatile plant blue-light receptors. *Trends Plant Sci. 7*, 204–210.

(14) Larsen, D. S., van Stokkum, I. H., Vengris, M., van Der Horst, M. A., de Weerd, F. L., Hellingwerf, K. J., and van Grondelle, R. (2004) Incoherent manipulation of the photoactive yellow protein photocycle with dispersed pump-dump-probe spectroscopy. *Biophys. J. 87*, 1858–1872.

(15) Tsuda, M., Nelson, B., Chang, C.-H., Govindjee, R., and Ebrey, T. G. (1985) Characterization of the chromophore of the third rhodopsin-like pigment of *Halobacterium halobium* and its photoproduct. *Biophys. J. 47*, 721–724.

(16) Kadori, H., Yoshihara, K., and Tokutomi, S. (1992) Primary process of phytochrome-initial step of photomorphogenesis in green plants. *J. Am. Chem. Soc. 114*, 10958–10959.

(17) Andel, F., Hasson, K. C., Gai, F., Anfinrud, P. A., and Mathies, R. A. (1997) Femtosecond time-resolved spectroscopy of the primary photochemistry of phytochrome. *Biospectroscopy 3*, 421–433.

(18) Muller, M. G., Lindner, I., Martin, I., Gartner, W., and Holzwarth, A. R. (2008) Femtosecond kinetics of photoconversion of the higher plant photoreceptor phytochrome carrying native and modified chromophores. *Biophys. J. 94*, 4370–4382.

(19) Swartz, T. E., Corchnoy, S. B., Christie, J. M., Lewis, J. W., Szundi, I., Briggs, W. R., and Bogomolni, R. A. (2001) The photocycle of a flavin-binding domain of the blue light photoreceptor phototropin. *J. Biol. Chem. 276*, 36493–36500.

(20) Crosson, S., and Moffat, K. (2002) Photoexcited structure of a plant photoreceptor domain reveals a light-driven molecular switch. *Plant Cell 14*, 1067–1075.

(21) Schleicher, E., Kowalczyk, R. M., Kay, C. W., Hegemann, P., Bacher, A., Fischer, M., Bittl, R., Richter, G., and Weber, S. (2004) On the reaction mechanism of adduct formation in LOV domains of the

plant blue-light receptor phototropin. *J. Am. Chem. Soc. 126*, 11067–11076.

(22) Alexandre, M. T. A., Domratcheva, T., Bonetti, C., van Wilderen, L., van Grondelle, R., Groot, M. L., Hellingwerf, K. J., and Kennis, J. T. M. (2009) Primary Reactions of the LOV2 Domain of Phototropin Studied with Ultrafast Mid-infrared Spectroscopy and Quantum Chemistry. *Biophys. J. 97*, 227–237.

(23) Harper, S. M., Neil, L. C., and Gardner, K. H. (2003) Structural basis of a phototropin light switch. *Science 301*, 1541–1544.

(24) Harper, S. M., Christie, J. M., and Gardner, K. H. (2004) Disruption of the LOV-Jα helix interaction activates phototropin kinase activity. *Biochemistry 43*, 16184–16192.

(25) Kottke, T., Heberle, J., Hehn, D., Dick, B., and Hegemann, P. (2003) Phot-LOV1: Photocycle of a blue-light receptor domain from the green alga *Chlamydomonas reinhardtii*. *Biophys. J. 84*, 1192–1201.

(26) Losi, A., Polverini, E., Quest, B., and Gartner, W. (2002) First evidence for phototropin-related blue-light receptors in prokaryotes. *Biophys. J. 82*, 2627–2634.

(27) Kennis, J. T., Crosson, S., Gauden, M., van Stokkum, I. H., Moffat, K., and van Grondelle, R. (2003) Primary reactions of the LOV2 domain of phototropin, a plant blue-light photoreceptor. *Biochemistry 42*, 3385–3392.

(28) Crosson, S., and Moffat, K. (2001) Structure of a flavin-binding plant photoreceptor domain: Insights into light-mediated signal transduction. *Proc. Natl. Acad. Sci. U.S.A. 98*, 2995–3000.

(29) Halavaty, A. S., and Moffat, K. (2007) N- and C-terminal flanking regions modulate light-induced signal transduction in the LOV2 domain of the blue light sensor phototropin 1 from *Avena sativa*. *Biochemistry 46*, 14001–14009.

(30) Nash, A. I., Ko, W. H., Harper, S. M., and Gardner, K. H. (2008) A conserved glutamine plays a central role in LOV domain signal transmission and its duration. *Biochemistry 47*, 13842–13849.

(31) Christie, J. M., Corchnoy, S. B., Swartz, T. E., Hokenson, M., Han, I. S., Briggs, W. R., and Bogomolni, R. A. (2007) Steric interactions stabilize the signaling state of the LOV2 domain of phototropin 1. *Biochemistry 46*, 9310–9319.

(32) Zoltowski, B. D., Vaccaro, B., and Crane, B. R. (2009) Mechanism-based tuning of a LOV domain photoreceptor. *Nat. Chem. Biol. 5*, 827–834.

(33) Freddolino, P. L., Nash, A. I., Harper, S. M., Gardner, K. H., and Schulten, K. (2011) Photoreaction-induced conformational changes in *A. sativa* Phot1-LOV2: A molecular dynamics study YYYmanuscript in preparation.

(34) Freddolino, P. L., Dittrich, M., and Schulten, K. (2006) Dynamic switching mechanisms in LOV1 and LOV2 domains of plant phototropins. *Biophys. J. 91*, 3630–3639.

(35) Dittrich, M., Freddolino, P. L., and Schulten, K. (2005) When light falls in LOV: A quantum mechanical/molecular mechanical study of photoexcitation in Phot-LOV1 of *Chlamydomonas reinhardtii*. *J. Phys. Chem. B 109*, 13006–13013.

(36) Nozaki, D., Iwata, T., Ishikawa, T., Todo, T., Tokutomi, S., and Kandori, H. (2004) Role of Gln1029 in the photoactivation processes of the LOV2 domain in adiantum phytochrome3. *Biochemistry 43*, 8373–8379.

(37) Fedorov, R., Schlichting, I., Hartmann, E., Domratcheva, T., Fuhrmann, M., and Hegemann, P. (2003) Crystal structures and molecular mechanism of a light-induced signaling switch: The Phot-LOV1 domain from *Chlamydomonas reinhardtii*. *Biophys. J. 84*, 2474–2482.

(38) Losi, A., Ghiraldelli, E., Jansen, S., and Gartner, W. (2005) Mutational effects on protein structural changes and interdomain interactions in the blue-light sensing LOV protein YtvA. *Photochem. Photobiol. 81*, 1145–1152.

(39) Humphrey, W., Dalke, A., and Schulten, K. (1996) VMD: Visual molecular dynamics. *J. Mol. Graphics 14* (33–38), 27–38.

(40) Phillips, J. C., Braun, R., Wang, W., Gumbart, J., Tajkhorshid, E., Villa, E., Chipot, C., Skeel, R. D., Kale, L., and Schulten, K. (2005) Scalable molecular dynamics with NAMD. *J. Comput. Chem. 26*, 1781–1802.

(41) Alexandre, M. T., Arents, J. C., van Grondelle, R., Hellingwerf, K. J., and Kennis, J. T. (2007) A base-catalyzed mechanism for dark state recovery in the *Avena sativa* phototropin-1 LOV2 domain. *Biochemistry 46*, 3129–3137.

(42) Iwata, T., Yamamoto, A., Tokutomi, S., and Kandori, H. (2007) Hydration and temperature similarly affect light-induced protein structural changes in the chromophoric domain of phototropin. *Biochemistry 46*, 7016–7021.

(43) Laan, W., Bednarz, T., Heberle, J., and Hellingwerf, K. J. (2004) Chromophore composition of a heterologously expressed BLUF-domain. *Photochem. Photobiol. Sci. 3*, 1011–1016.

(44) Farmer, B. T., Constantine, K. L., Goldfarb, V., Friedrichs, M. S., Wittekind, M., Yanchunas, J., Robertson, J. G., and Mueller, L. (1996) Localizing the NADP$^+$ binding site on the MurB enzyme by NMR. *Nat. Struct. Biol. 3*, 995–997.

(45) Mueller, F. (1991) *Chemistry and biochemistry of flavoenzymes*, CRC Press, Boca Raton, FL.

(46) Gauden, M., van Stokkum, I. H. M., Key, J. M., Luhrs, D. C., Van Grondelle, R., Hegemann, P., and Kennis, J. T. M. (2006) Hydrogen-bond switching through a radical pair mechanism in a flavin-binding photoreceptor. *Proc. Natl. Acad. Sci. U.S.A. 103*, 10895–10900.

(47) Wolf, M. M. N., Schumann, C., Gross, R., Domratcheva, T., and Diller, R. (2008) Ultrafast Infrared Spectroscopy of Riboflavin: Dynamics, Electronic Structure, and Vibrational Mode Analysis. *J. Phys. Chem. B 112*, 13424–13432.

(48) Stanley, R. J., and MacFarlane, A. W. (2000) Ultrafast excited state dynamics of oxidized flavins: Direct observations of quenching by purines. *J. Phys. Chem. A 104*, 6899–6906.

(49) Heelis, P. F., Parsons, B. J., Phillips, G. O., and Mckellar, J. F. (1981) The Flavin Sensitized Photo-Oxidation of Ascorbic-Acid: A Continuous and Flash-Photolysis Study. *Photochem. Photobiol. 33*, 7–13.

(50) Holzer, W., Penzkofer, A., Fuhrmann, M., and Hegemann, P. (2002) Spectroscopic characterization of flavin mononucleotide bound to the LOV1 domain of Phot1 from *Chlamydomonas reinhardtii*. *Photochem. Photobiol. 75*, 479–487.

(51) Salzmann, S., Silva, M. R., Thiel, W., and Marian, C. M. (2009) Influence of the LOV Domain on Low-Lying Excited States of Flavin: A Combined Quantum-Mechanics/Molecular-Mechanics Investigation. *J. Phys. Chem. B 113*, 15610–15618.

(52) Berberan-Santos, M. N. (2000) External heavy-atom effect on fluorescence kinetics. *Phys. Chem. Commun. 5*, 18–23.

(53) Chandra, A. K., Turro, N. J., Lyons, A. L., and Stone, P. (1978) Intra-Molecular External Heavy-Atom Effect in Bromonorbornenes, Benzonorbornenes and Naphthonorbornenes. *J. Am. Chem. Soc. 100*, 4964–4968.

(54) Alexandre, M. T. A., van Grondelle, R., Hellingwerf, K. J., Robert, B., and Kennis, J. T. M. (2008) Perturbation of the ground-state electronic structure of FMN by the conserved cysteine in phototropin LOV2 domains. *Phys. Chem. Chem. Phys. 10*, 6693–6702.

(55) Zoltowski, B. D., Schwerdtfeger, C., Widom, J., Loros, J. J., Bilwes, A. M., Dunlap, J. C., and Crane, B. R. (2007) Conformational switching in the fungal light sensor Vivid. *Science 316*, 1054–1057.

(56) Autrey, T., Devadoss, C., Sauerwein, B., Franz, J. A., and Schuster, G. B. (1995) Solvent Cage Recombination of 4-Benzoylphenylthiyl Radicals: Fast Intersystem Crossing of Triplet Sulfur-Centered Radical Pairs. *J. Phys. Chem. 99*, 869–871.

(57) van Stokkum, I. H., Larsen, D. S., and van Grondelle, R. (2004) Global and target analysis of time-resolved spectra. *Biochim. Biophys. Acta 1657*, 82–104.

(58) Holzwarth, A. R. (1996) in *Biophysical Techniques in Photosynthesis*, Chapter 5, pp 75–92, Kluwer, Dordrecht, The Netherlands.

(59) Zagrovic, B., and Pande, V. (2003) Solvent viscosity dependence of the folding rate of a small protein: Distributed computing study. *J. Comput. Chem. 24*, 1432–1436.

(60) Zirak, P., Penzkofer, A., Mathes, T., and Hegemann, P. (2009) Photo-dynamics of roseoflavin and riboflavin in aqueous and organic solvents. *Chem. Phys. 358*, 111–122.

(61) Alexandre, M. T. A., van Grondelle, R., Hellingwerf, K. J., and Kennis, J. T. M. (2009) Conformational Heterogeneity and Propagation of Structural Changes in the LOV2/Jα Domain from *Avena sativa* Phototropin 1 as Recorded by Temperature-Dependent FTIR Spectroscopy. *Biophys. J. 97*, 238–247.

(62) Bonetti, C., Mathes, T., van Stokkum, I. H. M., Mullen, K. M., Groot, M. L., van Grondelle, R., Hegemann, P., and Kennis, J. T. M. (2008) Hydrogen Bond Switching among Flavin and Amino Acid Side Chains in the BLUF Photoreceptor Observed by Ultrafast Infrared Spectroscopy. *Biophys. J. 95*, 4790–4802.

(63) Corchnoy, S. B., Swartz, T. E., Szundi, I., Lewis, J. W., Briggs, W. R., and Bogomolni, R. A. (2003) Proton transfers in the photocycle of the LOV2 domain of phototropin 1. *Biophys. J. 84*, 398A.

(64) Cohen, J., Arkhipov, A., Braun, R., and Schulten, K. (2006) Imaging the migration pathways for O_2, CO, NO, and Xe inside myoglobin. *Biophys. J. 91*, 1844–1857.

(65) Foote, C. S., and Peters, J. W. (1971) Chemistry of singlet oxygen: Reactive Intermediate in Sulfide Photooxidation. *J. Am. Chem. Soc. 93*, 3795.

(66) Schoneich, C., Aced, A., and Asmus, K. D. (1993) Mechanism of Oxidation of Aliphatic Thioethers to Sulfoxides by Hydroxyl Radicals: The Importance of Molecular Oxygen. *J. Am. Chem. Soc. 115*, 11376–11383.

(67) Massey, V. (2000) The chemical and biological versatility of riboflavin. *Biochem. Soc. Trans. 28*, 283–296.

(68) Chlumsky, L. J., Sturgess, A. W., Nieves, E., and Jorns, M. S. (1998) Identification of the covalent flavin attachment site in sarcosine oxidase. *Biochemistry 37*, 2089–2095.

(69) Steenkamp, D. J., Kenney, W. C., and Singer, T. P. (1978) Novel Type of Covalently Bound Coenzyme in Trimethylamine Dehydrogenase. *J. Biol. Chem. 253*, 2812–2817.

(70) Strickland, D., Yao, X. L., Gawlak, G., Rosen, M. K., Gardner, K. H., and Sosnick, T. R. (2010) Rationally improving LOV domain-based photoswitches. *Nat. Methods 7*, 623–626.